http://dx.doi.org/10.5012/bkcs.2013.34.7.1995

Preparation and Cyclic Performance of $Li_{1.2}(Fe_{0.16}Mn_{0.32}Ni_{0.32})O_2$ Layered Cathode Material by the Mixed Hydroxide Method

K. Karthikeyan, K. W. Nam,† E. Y. Hu,† X. Q. Yang,† and Y. S. Lee*

Faculty of Applied Chemical Engineering, Chonnam National University, Gwangju 500-757, Korea
**E-mail: leeys@chonnam.ac.kr*
†*Chemistry Department, Brookhaven National Laboratory, Upton, NY 11973, USA*
Received January 29, 2013, Accepted April 3, 2013

Layered $Li_{1.2}(Fe_{0.16}Mn_{0.32}Ni_{0.32})O_2$ was prepared by the mixed hydroxide method at various temperatures. X-ray diffraction (XRD) pattern shows that this material has a α-$NaFeO_2$ layered structure with $R\bar{3}m$ space group and that cation mixing is reduced with increasing synthesis temperature. Scanning electron microscopy (SEM) reveals that nano-sized $Li_{1.2}(Fe_{0.16}Mn_{0.32}Ni_{0.32})O_2$ powder has uniform particle size distribution. X-ray absorption near edge structure (XANES) analysis is used to study the local electronic structure changes around the Mn, Fe, and Ni atoms in this material. The sample prepared at 700 °C delivers the highest discharge capacity of 207 $mAhg^{-1}$ between 2-4.5 V at 0.1 $mAcm^{-2}$ with good capacity retention of 80% after 20 cycles.

Key Words : Mixed hydroxide method, Lithium Mn oxide, XANES, Layered materials, Lithium batteries

Introduction

Layered $LiCoO_2$ has been widely used as electrodes in commercial lithium batteries for such as mobile phones and portable computers. Increases of the operating voltage and capacity of lithium ion batteries are important to extending their application to hybrid electrical vehicles (HEV) and plug-in hybrid electric vehicles (PHEV). Layered lithium-rich mixed transition metal oxides composites with Li_2MnO_3 are good candidates for high capacity and high operating voltage applications.

Structurally integrated nano-composites of Li_2MnO_3 and $LiMO_2$ (M = Ni, Co and Cr) have been reported to form highly complex atomic arrangements in which Li_2MnO_3 domains with short-range order exist within a $LiMO_2$ matrix.[1-3] The extraction of two lithium ions from the Li_2MnO_3 during charging and the reinsertion of only one lithium ion per MnO_2 unit during discharge results in irreversible capacity loss during initial cycling. Compared with lithium metal oxides containing cobalt, nickel, and chromium, lithium-iron oxides have advantages in terms of reduced costs and toxicity. Of the several tested iron-based cathodes, $LiFeO_2$ is promising for lithium secondary batteries.[4,5] However, its disadvantages, including lower operating voltage, no electrochemical activity (especially, the cubic α,β-form), and poor cycling characteristics, strongly hamper its practical application. Therefore, advanced trials of lithium extraction from $LiFeO_2$ have used the $Fe^{3+/4+}$ redox couple, which has been observed in $LiFe_xM_{1-x}O_2$ (M = Co and Ni, $0 < x < 0.3$).[6,7] This material's capacity and reversibility decrease with increasing Fe content, indicating that the $LiFeO_2$ phase of the materials is less electrochemically active. Tabuchi *et al.* recently successfully reported the use of the $Fe^{3+/4+}$ redox couple at *ca.* 4 V through the substitution of Fe in Li_2MnO_3. $LiFeO_2$-Li_2MnO_3 was prepared by combined co-precipitation, hydrothermal processing, and calcination. It had a 4 V plateau on both charge and discharge. The changes in valence state between Fe^{3+} and Fe^{4+} were confirmed by *in situ* Fe Mössbauer spectroscopy.[8,9] Although this material could be prepared with suitable electrochemical properties, its synthesis was too complex to be useful. It involved three steps that could affect electrochemical performance and result in a low reproducibility of final powder. Their reported hydrothermal method was complicated and could significantly increase manufacturing costs. The mass-production of iron-based lithium batteries would benefit from the development of a simple and low cost alternate synthesis. In this connection, we tried to find out the possibilities of the preparation of layered materials by simple synthesis process and studied their charge discharge performances.

To develop new cathodes with good electrochemical properties, iron and nickel doped Li_2MnO_3 ($Li_{1+x}(Mn_{0.4}Fe_{0.2}Ni_{0.4})_{1-x}O_2$, $0 < x < 0.4$) with three end member of Li_2MnO_3, $LiNiO_2$ and $LiFeO_2$ were prepared by a simple mixed hydroxide method. Although the optimization of x value did not presented in this work, the material prepared at $x = 0.2$ [$Li_{1.2}(Fe_{0.16}Mn_{0.32}Ni_{0.32})O_2$] exhibited the best electrochemical properties in all samples. This paper reports the effects of calcination temperature on the performance and structure of $Li_{1.2}(Fe_{0.16}Mn_{0.32}Ni_{0.32})O_2$ cathodes for lithium ion batteries. The samples' structural and electrochemical properties were investigated by XANES analysis.

Experimental

The iron and nickel-doped Li_2MnO_3 [$Li_{1.2}(Fe_{0.16}Mn_{0.32}Ni_{0.32})O_2$] was prepared by the mixed hydroxide method followed by calcination at various temperatures. LiOH (Jensei Chem., Japan), $Fe(NO_3)_3{\cdot}9H_2O$ (Jensei Chem., Japan), $MnCl_2{\cdot}4H_2O$ (Wako, Japan) and $Ni(NO_3)_3{\cdot}6H_2O$ (Jensei

Chem., Japan) were used as starting materials. Stoichiometric amounts of the transition metal salts were dissolved in distilled water and cooled to −10 °C to suppress spinel ferrite formation, which could affect the material's electrochemical performance. Aqueous LiOH was added to the cooled metal solution to obtain a mixed Ni, Mn and Fe hydroxide solution, which was aged for 12 h. It was then filtered, washed to remove residual Li salts and dried at 60 °C for 10 h in air. The final products were obtained by firing the precipitate with excess LiOH at different temperatures for10h under an oxygen flow.

Powder X-ray diffraction (XRD, Rint 1000, Rigaku, Japan) using CuKα radiation determined the samples' crystalline phases. Rietveld refinement of the collected XRD data were made using GSAS-EXPGUI.[10,11] Particle morphologies and size distributions were analyzed by scanning electron microscopy (FE-SEM, S-4700, Hitachi, Japan). X-ray absorption spectra (XAS) at Mn, Fe, and Ni K-edges were collected in transmission mode on Beamline X18A at the National Synchrotron Light Source (NSLS) at Brookhaven National Lab. (BNL, USA) using a Si(111) double-crystal mono chromator. The beam intensity was reduced by 30% to minimize high order harmonics. Reference spectra of each element for energy calibration were simultaneously collected using Mn, Fe, and Ni metal foils. The measured spectra were normalized using a standard algorithm of pre-edge subtraction and edge-step normalization.[12] The chemical stoichiomettry of the prepared samples was calculated using atomic emission spectrometer (Perkin Elmer, OPTIMA 4300 DV). Charge-discharge testing was performed using CR2032 type cells. The cells' cathodes were prepared by pressing a slurry of 20 mg prepared material, 3 mg Ketzen black and 3 mg Teflonized acetylene black (TAB) on a 200 mm^2 stainless steel mesh current collector at a pressure of 300 $kgcm^{-2}$ and drying at 160 °C for 5 h in a vacuum oven. The test cells comprised a cathode and a lithium metal anode separated by a porous polypropylenefilm (Celgard 3401). The electrolyte was a mixture of 1 M $LiPF_6$-ethylene carbonate (EC)/dimethyl carbonate (DMC) (1:1 by vol., Techno Semichem Co., Ltd, Korea). Cyclic voltammetry (CV) study was performed using an electrochemical analyzer (SP-150, Bio-Logic, France). The charge and discharge current densities were both 0.1 $mAcm^{-2}$ with cut-off voltages of 2.0 to 4.5 V at room temperature.

Results and Discussion

The XRD patterns of $Li_{1.2}(Fe_{0.16}Mn_{0.32}Ni_{0.32})O_2$ prepared at different calcination temperatures are similar to $Li_{2-x}MnO_{3-x/2}$ ($R\bar{3}m$) rather than stoichiometric Li_2MnO_3(monoclinic, $C2/m$, Figure 1). They show no impurity peaks representing Li_2CO_3, $LiMnO_2$, NiO and α-$LiFeO_2$. All the XRD patterns could be indexed with α-$NaFeO_2$ unit cell with $R\bar{3}m$ space group. Small, unindexed peaks between 20 and 25° were commonly observed in the patterns, which are characteristic super lattice peaks of Li_2MnO_3. Such peaks have been reported to originate from sublattice ordering of Li^+ and

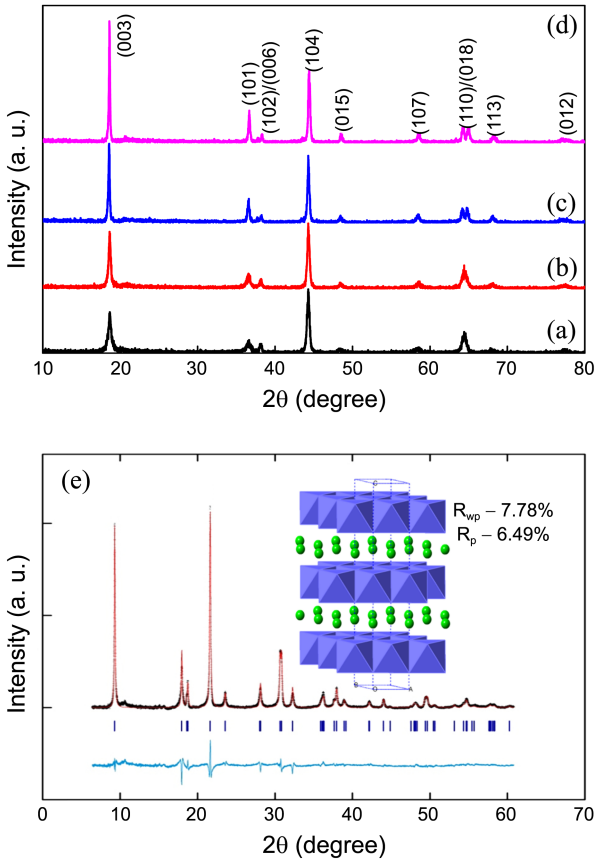

Figure 1. XRD patterns of $Li_{1.2}(Fe_{0.16}Mn_{0.32}Ni_{0.32})O_2$ prepared at different calcination temperatures. (a) 650 °C, (b) 700 °C, (c) 750 °C, (d) 800 °C, and (e) Rietveld analysis of the sample prepared at 700 °C.

transitional metal ions in the layers predominantly containing transitional metal ions with additional Li^+.[13] The lattice constants, a and c, c/a ratios, and $I_{(003)}/I_{(104)}$ ratios of the hexagonal unit cells are listed in Table 1. The values of a_h and c_h (lattice constants for the hexagonal unit cell) decreased slightly with increasing calcination temperature. Rougier *et al.*[14] suggested that splitting of the (006)/(012) and (108)/(110) doublets indicates the formation of a highly ordered layered structure. As temperature increased, the separation of the (006)/(012) and (108)/(110) peaks became more pronounced, indicating increased ordering of the layered structure. It has been reported that with increasing c/a ratio beyond 4.90, the ordering of the layered structure increases and the crystal structure becomes more hexagonal.[15,16] In this study, the c/a values of all the samples were

Table 1. Lattice parameters of $Li_{1.2}(Fe_{0.16}Mn_{0.32}Ni_{0.32})O_2$ samples obtained at different calcination temperatures

Temperature (°C)	a_h (nm)	c_h (nm)	c/a	$I_{(003)}/I_{(104)}$
650	2.887	14.283	4.92	0.76
700	2.881	14.276	4.92	0.98
750	2.874	14.254	4.93	1.05
800	2.870	14.243	4.96	1.15

more than 4.90, indicative of pronounced layered structures. The intensity ratio $I_{(003)}/I_{(104)}$ is an effective indicator of the disorder of the cations in the lattice, with higher ratios representing lower degrees of cation mixing. This intensity ratio linearly increased with increasing calcination temperature, implying that increased calcination temperatures facilitated better layering of the structures and reduced cation mixing. High crystallinity is an important factor for good electrochemical cycling performance and structural stability during cycling.

In order to find out the cation disordering in sample prepared with mixed hydroxide method, the XRD pattern of sample calcined at 700 °C was examined by Rietveld refinement and the result is showed in Figure 1(e). The refinement profile fitting was done based on the assumption of occupancy of Li ion in 3a site; metal ions are in 3b site and O atoms in 6c site. The fitted structure for sample calcined at 700 °C based on α-$NaFeO_2$ type with $R\bar{3}m$ space group was shown as inset in Figure 1(e). The lithium ions and transition metal ions occupy alternating layers in a cubic close packed framework of oxygen, which correspond to 3a and 3b site. The difference between calculated and experimental patterns is very small and the low agreement parameter values (R_{wp} and R_p) demonstrated a successful refinement. As can be seen from the good minimization of the differences, at least the long-range structure is well described by the model. It is also clear that the appearance of superstructure peaks around 20° to 30° could be assigned to the Li and Mn ion ordering in the transition metal layers.[14,17] According to Rietveld analysis, the refinement indicated only 0.08 unit mole of Ni^{2+} from 3b site incorporate into the lithium layer, giving a final composition $(Li_{0.920}Ni^{2+}_{0.08})_{3a}(Li_{0.280}, M_{0.720})_{3b}O_2$ where M stands for transition metals (Mn, Ni and Fe). This clearly revealed that only lower amount of cation disordering occurred for sample calcined at 700 °C. The chemical compositions of the samples calcined at different temperatures were calculated using ICP analysis and the results were presented in Table 2. As seen from the Table 2, the calculated values are closely matched with the expected ratio of $Li_{1.2}(Fe_{0.16}Mn_{0.32}Ni_{0.32})O_2$. The variation in lithium content may be due to lithium loss at the high temperature calcination.

The morphologies of the samples are shown in Figure 2. All particles appeared to comprise aggregates of submicrometer particles. As expected, the particles' sizes increased with increasing temperature. Their crystallinities also increased with increasing temperature. At calcination temperatures up to 750 °C, particle sizes gradually increased from 60 nm to 150 nm with unchanged particle shapes. However, at

Table 2. Chemical composition of $Li_{1.2}(Fe_{0.16}Mn_{0.32}Ni_{0.32})O_2$ samples obtained by ICP analysis

Elements	650 °C	700 °C	750 °C	800 °C
Li	1.09	1.15	1.14	1.12
Mn	0.319	0.319	0.321	0.32
Fe	0.155	0.158	0.155	0.154
Ni	0.318	0.317	0.321	0.316

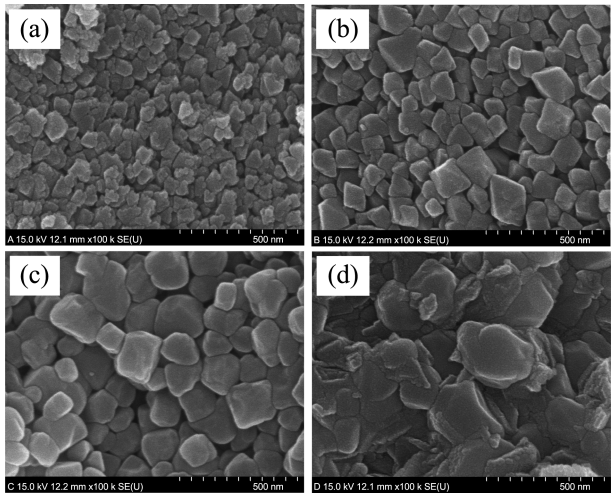

Figure 2. SEM images of $Li_{1.2}(Fe_{0.16}Mn_{0.32}Ni_{0.32})O_2$ prepared at (a) 650 °C, (b) 700 °C, (c) 750 °C, and (d) 800 °C.

800 °C, particle sizes rapidly increased and their shapes changed greatly. This is generally due to the agglomeration of particles at 800 °C, however, the parameters listed in Table 1, such asthe ratios of c/a and $I_{(003)}/I_{(104)}$, clearly indicated some structural changes as the calcination temperature reached 800 °C. Although the sample calcined at 800 °C showed the best layered hexagonal structure from the XRD patterns, it was not the best material in terms of the discharge capacity, which will be discussed further below.

Figure 3 shows initial charge/discharge profiles of the Li/$Li_{1.2}(Fe_{0.16}Mn_{0.32}Ni_{0.32})O_2$ cells obtained at different calcination temperatures. These cells were charged and discharged at a current density of 0.1 $mAcm^{-2}$ between 2 and 4.5 V. The charging profiles of all the samples start at the cell open circuit potential and monotonically rapidly increased to 3.7 V and then holds at 3.8 V where the oxidation of Ni^{2+} to Ni^{4+}

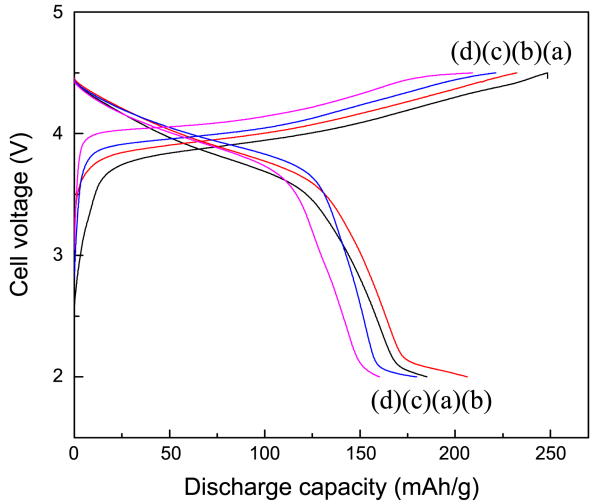

Figure 3. Initial charge/discharge curves of Li/$Li_{1.2}(Fe_{0.16}Mn_{0.32}Ni_{0.32})O_2$ prepared at different calcination temperatures. (a) 650 °C, (b) 700 °C, (c) 750 °C, and (d) 800 °C. These cells were charged and discharged at a current density of 0.1 $mAcm^{-2}$ between 2.0 and 4.5 V.

occurred.[18] Above 4.45 V, a voltage plateau was observed, mainly due to the electrochemical removal of Li_2O associated with the irreversible loss of oxygen from the lattice.[19] Moreover, it was believed that the oxidation limitation for Mn^{4+} to form Mn^{5+} was believed to restrict the participation of Mn^{4+} during electrochemical reaction.[20] Similarly, Fe^{3+} is also not oxidized in to Fe^{4+} and subsequent reduction during discharge. Thus it is possibly assumed that Mn^{4+} and Fe^{3+} are inactive members and helps in stabilizing the crystal structure of $Li_{1.2}(Fe_{0.16}Mn_{0.32}Ni_{0.32})O_2$ solid solution during intercalation/de-intercalation.[9,20] All samples showed smooth discharge curves until *ca.* 3.5 V, at which their gradients became much steeper. A further change, a flattening of gradient, was also observed between 2.25-2 V. The origins of these changes of gradient are not clearly understood; similar tendencies have been reported elsewhere.[21] The irreversible capacity losses of all the samples likely resulted from the formation of inactive regions due to the oxidation of Ni^{2+} ions occupying Li sites in the Li layer.[22] The sample calcined at 700 °C delivered the maximum discharge capacity of all the samples (207 $mAhg^{-1}$ in the first cycle), whereas the material prepared at 800 °C delivered the lowest discharge capacity (160 $mAhg^{-1}$). The discharge capacities of the samples prepared at 650 and 750 °C were *ca.* 185 and 180 $mAhg^{-1}$ respectively. Of the four samples, that prepared at 800 °C had the lowest capacity, despite having the best layered structure.

XAS is an element-selective and powerful tool to investigate the electronic and local geometric structures of lithiated ternary-transition-metal oxides. Therefore, X-ray absorption near edge structure (XANES) analyses were carried out to compare changes of local structure around the Mn, Fe, and Ni atoms in $Li_{1.2}(Fe_{0.16}Mn_{0.32}Ni_{0.32})O_2$ samples. Figure 4 shows the Mn, Fe and Ni K-edge XANES spectra of $Li_{1.2}(Fe_{0.16}Mn_{0.32}Ni_{0.32})O_2$ together with those of some reference compounds which have known oxidation states. All spectra display two important pre-edge and main absorption features, labeled A and B in Figure 4. The insets show enlargements of the region of the pre-edge peak, A. The weak pre-edge absorption peaks can be assigned to the electronic excitation of 1s core electrons to unoccupied 3d orbitals of the transition metal ions. This 1s → 3d transition is formally electric dipole forbidden in ideal octahedral symmetry. The appearance of this weak absorption peak is due to 3d-4p orbital mixing arising from the non centrosymmetric environment of the slightly distorted octahedral 3a site in the rhombohedral $R\bar{3}m$ space group.[23-25] Therefore, this pre-edge peak can provide useful information about the site symmetry, degree of distortion in the octahedra and the oxidation state of the core atoms. The main absorption peaks, B, are due to pure dipole-allowed transitions of 1s core electrons to unoccupied 4p bound states without shakedown processes.[23-25]

The Mn K-edge spectra in Figure 4(a) are almost identical to the Mn^{4+} reference spectrum of $Li[Ni_{1/3}Co_{1/3}Mn_{1/3}]O_2$ and were unchanged with respect to calcination temperature, implying that the local structure around the Mn atoms did not vary greatly and that the Mn ions existed mostly as Mn^{4+} in all the samples regardless of calcinations temperature. The Fe K-edge spectra show the edge positions of the $Li_{1.2}(Fe_{0.16}Mn_{0.32}Ni_{0.32})O_2$ samples lying closer to the α-$LiFeO_2$ (Fe^{3+}) spectrum than the Fe_3O_4 ($Fe^{2.67+}$) spectrum (Fig. 4(b)), indicating the trivalent oxidation state of iron ions in all of this compound.[26,27] The slight shift in edge position does not affect the valence state of ions.[28] The ridge edge does not shift with calcination temperature, indicating that most of the Fe atoms were present as Fe^{3+} in the $Li_{1.2}(Fe_{0.16}Mn_{0.32}Ni_{0.32})O_2$.[26] All the materials exhibited a pre-edge peak around ~7115 eV in Figure 4(b), which is assigned as the dipole-forbidden 1s → 3d transition.[27] The very weak intensities of the pre-edge peaks indicate that the Fe atoms were in octahedral coordination, as the pre-edge peaks associated with tetrahedral coordination are more intense, as demonstrated by the pre-edge peak of Fe_3O_4, where 1/3 of the Fe atoms occupy tetrahedral sites (inset in Fig. 4(b)). However, it should be noted that the pre-edge intensity slightly increased as calcination temperature increased from 750 to 800 °C, suggesting increased local structural distortion in the Fe-O_6

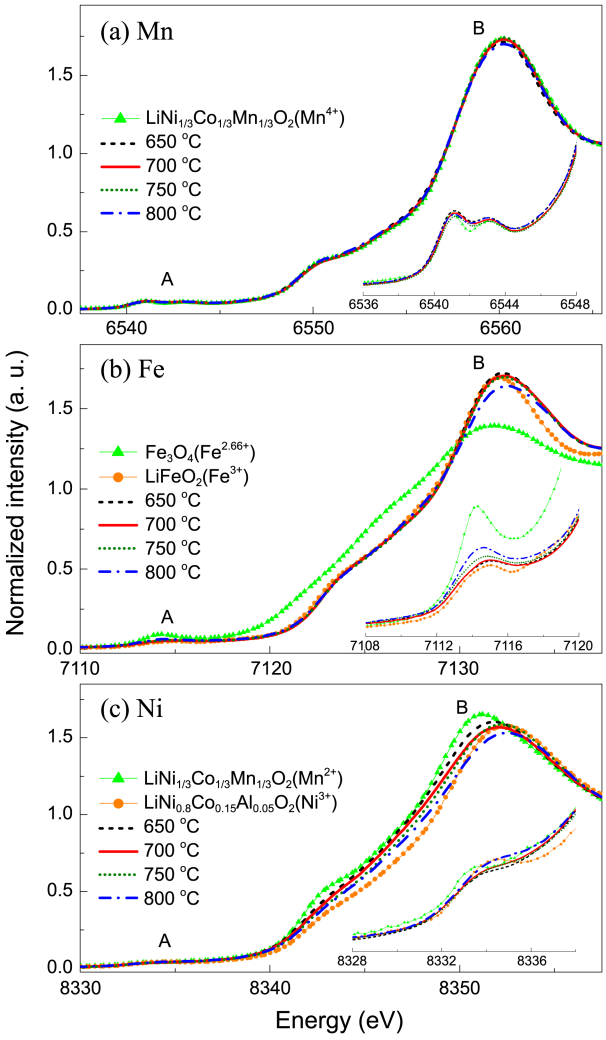

Figure 4. (a) Mn, (b) Fe, and (c) Ni K-edge XANES spectra of $Li_{1.2}(Fe_{0.16}Mn_{0.32}Ni_{0.32})O_2$ prepared at different calcination temperatures.

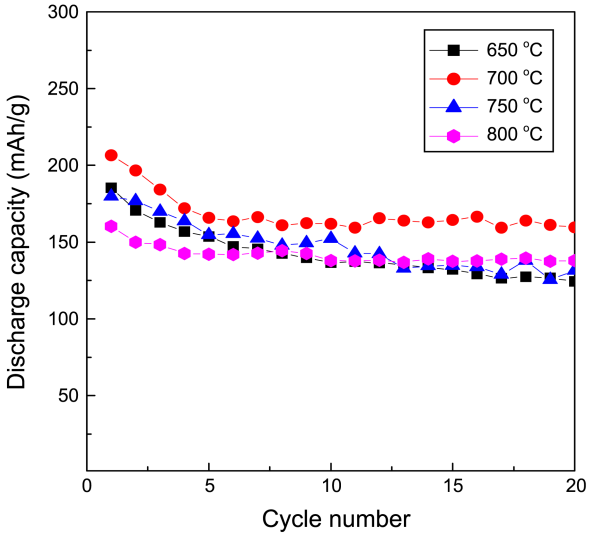

Figure 5. Cycle performance of $Li/Li_{1.2}(Fe_{0.16}Mn_{0.32}Ni_{0.32})O_2$ prepared at different calcination temperatures. The cells were charged and discharged at a current density of 0.1 $mAcm^{-2}$ between 2.0 and 4.5 V.

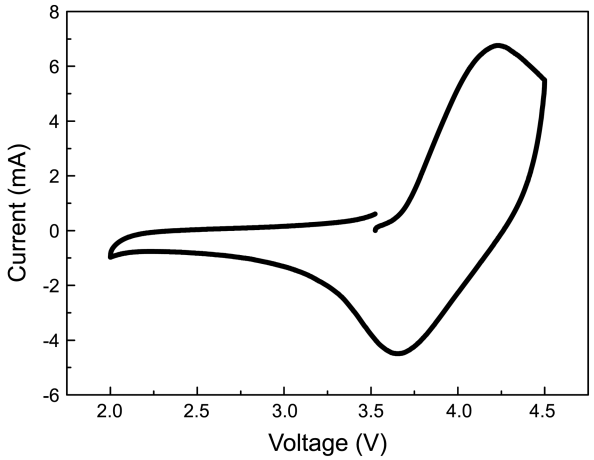

Figure 6. CV trace of the cell containing $Li_{1.2}Mn_{0.32}Ni_{0.32}Fe_{0.16}O_2$ electrode synthesized using mixed hydroxide method at 700 °C. The CV was recorded at 0.2 mVs^{-1} scan rate between 2-4.5 V.

octahedra at temperatures ≥ 750 °C. In contrast to the Mn and Fe K-edge spectra, the Ni K-edge spectra (Fig. 4(c)) show a rigid edge shift toward higher energies with increasing calcination temperatures from 650 to 800 °C. Comparison with the edge positions of the $LiNi_{1/3}Co_{1/3}Mn_{1/3}O_2$ (Ni^{2+}) and $LiNi_{0.8}Co_{0.15}Al_{0.05}O_2$ (Ni^{3+}) reference oxides demonstrates that the oxidation state of Ni at 650 °C was slightly over Ni^{2+} and continuously increases towards Ni^{3+} with increasing calcination temperature. A slight increase in the pre-edge peak intensity of the spectrum of the sample calcined at 800 °C was observed (inset of Fig. 4(c)) and this is attributable to increased local structural distortion of the Ni-O_6 octahedra due to the increased amount of Jahn-Teller active Ni^{3+} ions. There is a clear difference of nickel oxidation state between the three samples calcined at lower temperatures and the one calcined at 800 °C. The XANES results suggest the sample prepared at 800 °C delivered the lowest discharge capacity due to the higher initial oxidation state of Ni ions, close to Ni^{3+}, which limits the use of $Ni^{2+/4+}$ redox reactions during charging and discharging.

Figure 5 shows the effect of calcination temperature on the cycling performances of the $Li/Li_{1.2}(Fe_{0.16}Mn_{0.32}Ni_{0.32})O_2$ cells. All cells commonly demonstrated continuous capacity fading in the early cycles. It is well known that the electrochemical lithium insertion/extraction process very depends on particle size and the degree of agglomeration. It is also reported that crystalline materials with grain size of ~100 nm could exhibit enhanced diffusivity and higher thermal coefficient than conventional materials.[29] The sample calcined at 700 °C showed large capacity fading, while the one obtained at 800 °C exhibited much better cycle retention. Capacity retention rates after 20 cycles were 80% and 86% for the samples calcined at 700 °C and 800 °C, respectively. The capacity retention of the samples prepared at 650 °C and 750 °C are found to 67 and 73% after 20th cycle, respectively. This difference may be due to cation mixing and the degree of crystallinity, as determined from the XRD and SEM studies. Although the material prepared at 800 °C delivered low capacity, its capacity retention rate was the highest of all the samples. This is attributable to its well-developed layered structure and large particle sizes that can maintain structural stability better than the others can during cycling, despite its low initial discharge capacity.

In order to further understand the reaction mechanism of the sample calcined at 700 °C, CV study had taken between 2-4.5 V at 0.2 $mAcm^{-2}$ and the corresponding curve was presented in Figure 6. It can be seen from the CV curve that sample had only one major peak at ~4.2 V during the charging and at ~3.6 V during the discharging process. These peaks are attributed to the redox reaction of Ni^{2+}/Ni^{4+} couple as was speculated elsewhere.[30,31] It is worthy to mention here that, in order to maintain the charge neutrality, most of the Ni ions are presented in 2^+ oxidation state in $Li_{1.2}(Mn_{0.32}Ni_{0.32}Fe_{0.16})O_2$ sample.[32] Furthermore, the absence of redox peak ~3 V suggested that Mn ions are electrochemically inactive and are presented in Mn^{4+} state in all samples.[33] In addition, no transition of $Fe^{3+/4+}$ is observed at around 4 V throughout the region tested, which clearly revealing that Mn and Fe are electrochemically inactive and are mostly acted as activator to stabilize the $Li_{1.2}(Mn_{0.32}Ni_{0.32}Fe_{0.16})O_2$ structure during the electrochemical reaction. This result correlated well with the charge discharge studies as illustrated in Figure 3.

Conclusion

$Li_{1.2}(Fe_{0.16}Mn_{0.32}Ni_{0.32})O_2$ was prepared by the hydroxide method at different calcination temperatures. XRD studies showed that the samples had well-defined layered structures. The degree of crystallinity increased with increasing calcination temperature. All particles had uniform shapes and submicron size distributions. Of the samples tested, $Li_{1.2}(Fe_{0.16}Mn_{0.32}Ni_{0.32})O_2$ prepared at 700 °C delivered the

highest capacity of 207 $mAhg^{-1}$ and maintained 80% of the initial discharge capacity after 20 cycles. Although the material prepared at 800 °C delivered a lower capacity, it exhibited good capacity retention during cycling due to its better structural integrity.

Acknowledgments. This work was supported by Priority Research Centers Program through the National Research Foundation of Korea (NRF) funded by the Ministry of Education, Science and Technology (2009-0094055). Also, the work at BNL was supported by the Assistant Secretary for Energy Efficiency and Renewable Energy, Office of Vehicle Technologies, under the program of "Hybrid and Electric Systems", of the U. S. Department of Energy under Contract Number DEAC02-98CH10886.

References

1. Ammundsen, B.; Paulsen, J. *Adv. Mater.* **2001**, *13*, 943.
2. Lu, Z.; Dahn, J. R. *J. Electrochem. Soc.* **2003**, *150*, A1044.
3. Kang, S.-H.; Johnson, C. S.; Vaughey, J. T.; Amine, K.; Thackeray, M. M. *J. Electrochem. Soc*. **2006**, *153*, A1186.
4. Thackeray, M. M.; David, W. I. F.; Goodenough, J. B. *Mater. Res. Bull.* **1982**, *17*, 785.
5. Tabuchi, M.; Ado, K.; Sakaebe, H.; Masquelier, C.; Kageyama, H.; Nakamura, O. *Solid State Ionics* **1995**, *79*, 220.
6. Alcántara, R.; Jumas, J. C.; Lavela, P.; Fourcade, J. O.; Vicente, C. P.; Tirado, J. L. *J. Power Sources* **1999**, *81-82*, 547.
7. Reimers, J. N.; Rossen, E.; Jones, C. D.; Dahn, J. R. *Solid State Ionics* **1993**, *61*, 335.
8. Tabuchi, M.; Nabeshima, Y.; Ado, K.; Shikano, M.; Kageyama, H.; Tatsumi, K. *J. Power Sources* **2007**, *174*, 554.
9. Tabuchi, M.; Nabeshima, Y.; Takeuchi, T.; Kageyama, H.; Tatsumi, K.; Akimoto, J.; Shibuya, H.; Imaizumi, J. *J. Power Sources* **2011**, *196*, 3611.
10. Larson, A. C.; Von Dreele, R. B. *Los Alamos National Laboratory Report*; *LAUR*: 2000; p 86.
11. Toby, B. H. *J. Appl. Cryst.* **2001**, *34*, 210.
12. Sayers, D. E.; Bunker, B. A. In *X-Ray Absorption: Principles, Applications, Techniques of EXAFS, SEXAFS, and XANES*; Vol. 92 of *Chemical Analysis*, Koningsberger, D., Prins, R., Eds.; John Wiley and Sons: New York, 1988; Chap. 6, p 443.
13. Lu, Z.; Dahn, J. R. *J. Electrochem. Soc*. **2002**, *149*, A815.
14. Weill, F.; Tran, N. *et al*., *Electrochem. Solid-State Lett.* **2007**, *10*, A194.
15. Rougier, A.; Gravereau, P.; Delmas, C. *J. Electrochem. Soc.* **1996**, *143*, 1168.
16. Ammundsen, B.; Paulsen, J.; Davidson, I.; Liu, R. S.; Shen, C. H.; Chen, J. M.; Jang, L. Y.; Lee, J. F. *J. Electrochem. Soc.* **2002**, *149*, A431.
17. Paulsen, J. M.; Thomas, C. L.; Dahn, J. R. *J. Electrochem. Solid-State Lett.* **2000**, *147*, 861.
18. Koyama, Y.; Tanaka, I.; Adachi, H.; Makimura, Y.; Ohzuku, T. *J. Power Sources* **2003**, *119*, 644.
19. Lu, Z.; MacNeil, D. D.; Dahn, J. R. *Electrochem. Solid State Lett.* **2001**, *4*, A191.
20. Ammundsen, B. *J. Paulsen, Adv. Mater.* **2001**, *13*, 943.
21. Tabuchi, M.; Nabeshima, Y.; Takeuchi, T.; Tatsumi, K.; Imaizumi, J.; Nitta, Y. *J. Power Sources* **2010**, *195*, 834.
22. Delmas, C.; Menetrier, M.; Croguennec, L.; Saadoune, I.; Rougier, A.; Pouillerie, C.; Prado, G.; Grune, M.; Fournes, L. *Electrochim. Acta* **1999**, *45*, 243.
23. Kim, M. G.; Yo, C. H. *J. Phys. Chem. B* **1999**, *103*, 6457.
24. Kim, M. G.; Shin, H. J.; Kim, J. H.; Park, S. H.; Sun, Y. K. *J. Electrochem. Soc.* **2005**, *152*, A1320.
25. Yoon, W. S.; Grey, C. P.; Balasubramanian, M.; Yang, X. Q.; McBreen, J. *Chem. Mater.* **2003**, *15*, 3161.
26. Kim, T. W.; Ha, H. W.; Paek, M. J.; Hyun, S. H.; Baek, I. H.; Choy, J.-H.; Hwang, S. J. *J. Phys. Chem. C* **2008**, *112*, 14853.
27. Wooa, M. A.; Kima, T. W.; Kima, I. Y.; Hwang, S. J. *Solid State Ionics* **2011**, *182*, 91.
28. Combarieu, G.; Hamelet, S.; Millange, F.; Morcrette, M.; Tarascon, J. M.; Ferey, G.; Walton, R. I. *Electrochem. Comm.* **2009**, *11*, 1881.
29. Suryanarayana, C.; Koch, C. C. *Hyperfine Interact.* **2000**, *130*, 5.
30. Karthikeyan, K.; Amaresh, S.; Lee, G. W.; Aravindan, V.; Kim, H.; Kang, K. S.; Kim, W. S.; Lee, Y. S. *Electrochim. Acta* **2012**, *68*, 246.
31. Lu, Z.; Beaulieu, L. Y.; Donaberger, R. A.; Thomas, C. L.; Dahn, J. R. *J. Eleclectrochem. Soc.* **2002**, *6*, A778**.**
32. Kang, S. H.; Kim, J.; Stoll, M. E.; Abraham, D.; Sun, Y. K.; Amine, K. *J. Power Sources* **2002**, *112*, 41.
33. Wu, F.; Wang, M.; Su, Y.; Bao, L.; Chen, S. *J. Power Sources* **2010**, *195*, 2362.